Chalcogenide Letters Vol. 22, No. 7, July 2025, p. 625 - 636

Synthesis and photocatalytic performance of ZnS nanoparticles via electrospinning assisted hydrothermal technique

T. L. Yang [a], P. Y. Lin [b], Y. S. Fu [c], C. Y. Luo [c], K. C. Hsu [a,*]

[a] *Department of Marine Engineering, National Kaohsiung University of Science and Technology, Kaohsiung 805, Taiwan*

[b] *Department of Photonics, National Cheng Kung University, Tainan 701, Taiwan*

[c] *Department of Greenergy, National University of Tainan, Tainan 700, Taiwan*

In this study, high-crystallinity zinc sulfide (ZnS) at the nanoscale was synthesized using a combination of electrospinning and hydrothermal techniques. Initially, polyvinyl butyral (PVB)/ZnS composite nanofibers were fabricated via electrospinning. Subsequently, a hydrothermal reaction was employed to induce a dissolution-recrystallization mechanism, enabling the gradual formation of highly crystalline ZnS nanoparticles. The structural, morphological, and compositional characteristics of the ZnS nanoparticles were analyzed using scanning electron microscopy (SEM), X-ray diffraction (XRD), transmission electron microscopy (TEM) and energy-dispersive X-ray spectroscopy (EDS). Finally, the photocatalytic activity of three different ZnS materials—synthesized via electrospinning, hydrothermal treatment, and hydrothermal-assisted electrospinning—were performed by degradation of methylene blue (MB) under visible light irradiation. This investigation aimed to elucidate the correlation between nanoscale structure, crystallinity, and photocatalytic performance.

(Received March 14, 2025; Accepted July 15, 2025)

Keywords: Zinc sulfide, Nanocrystalline, Photocatalytic degradation, Electrospinning, Hydrothermal

1. Introduction

With the development of science and technology, semiconductor ceramic materials are widely used in our daily lives. Common semiconductor ceramic materials include ZnO [1-3], TiO_2 [4-6], SnO_2 [7-9], WO_3 [10, 11], In_2O_3 [12, 13], ZnS [14, 15] and CdS [15, 16], etc. Among them, II−VI semiconductor compound Zinc sulfide (ZnS), has drawn much attention, due to its excellent properties of luminescence [17,18], wide band gap [19,20], and general good film properties. For these benefits, ZnS has applications in light emitting diodes [21, 22], phosphors [23, 24], catalysts [25], and solar cells [26]. Solar energy is an inexhaustible and sustainable resource. Therefore, efficient utilize of light is an essential prerequisite for using of solar energy. The solar water heaters, photovoltaics, and photocatalytic reactions illustrate the solar energy conversion into heat or electricity has been studied extensively. Various materials with semiconducting effect have been widely applied as energy conversion and optical application. ZnS has two crystal phases, among which the wurtzite (hexagonal) structure is a high-temperature stable phase, and the sphalerite (cubic sphalerite) structure is a low-temperature stable phase [27, 28]. The bandgap energies (Eg)

* Corresponding author: kchsu@nkust.edu.tw

https://doi.org/10.15251/CL.2025.227.625

at room temperature are 3.91 eV and 3.68 eV, respectively [29]. For $CuInGaSe_2$ (CIGS) thin film based solar cells, ZnS has been used to replace cadmium sulfide (CdS) as buffer layer, because zinc is non-toxicant and friendly to the environment than cadmium. Meanwhile, the wider band gap material of ZnS can be used to replace CdS (Eg=2.4 eV), which could lead to a decrement of window absorption losses and transmitting higher energy photons [30, 31].

It is important to note that photocatalytic activity depends not only on the energy gap but also on particle size, structure, and crystallinity. In particular, crystallinity plays a crucial role, as the recombination of photogenerated electrons and holes poses a significant challenge. For efficient photocatalysis, especially in water splitting, a high degree of crystallinity is generally preferred over a large surface area to minimize recombination and enhance performance [32]. In general, surface area decreases with increasing particle size and crystalline quality, which is a negative factor. Generally speaking, the higher the quality of the crystal, the fewer defective structures there will be, which usually leads to a better particle growth. If the materials which can be prepared with nanoscale and high crystallinity quality that must can give the photo-splitting studies a “shot in the arm”.

Many routes such as chemical vapor deposition (CVD) [33], thermal evaporation [34], sol-gel [35], electrospinning process [36], and the solvothermal method [37] have been used to synthesize ZnS nanomaterials. At present, solvothermal method is widely used as a functional method for preparation of nanomaterials. Furthermore, one-dimensional nanofibers fabricated through a straightforward electrospinning process can yield a variety of synthetic fibers, demonstrating significant potential for practical applications. Li et al. [38] changed the molar ratio of the reactants to synthesis of ZnS with different structures and morphologies. Liu et al. [39] prepared the ZnS hollow spheres with nano- and submicro-sizes through a facile template-free route. Biswas et al. [40] used the solvothermal process with different solvents to synthesize the ZnS nanostructures and control their shape and phase. Chai et al. [41] synthesized the bundles of wurtzite ZnS nanowires by solvothermal method. Lin et al. [36] using the ZnO nanofibers prepared via electrospinning process as a template, then thermal treatment in a H_2S atmosphere at 500 °C to obtain the nanostructured ZnS. Zhou et al. [42] obtained hybridize composites, ZnS nanoparticles which are dispersed in the surface of PVA nanofibers via electrospinning technique and then introducing zinc ions and sulfide ions to coordinate with carboxylic PVA nanofibers. In this study, we fabricate ZnS with both nanoscale and high crystalline quality, namely “dissolution-recrystallization” mechanism [43]. Unlike other technique which hired toxic gas H_2S for the further sulfurization processes to form ZnS nanofibers, the ZnS/PVB composite nanofibers were already formed in electrospinning process in this work. The electrospun ZnS/PVB nanofibers were further employed to fabricate ZnS nanomaterials by hydrothermal technique. A simple and novel method is used to prepare ZnS with both nanoscale and high crystalline quality which is essential for photocatalytic activity factors. It can be seen that ZnS nanoparticles prepared using this method exhibit good photocatalytic activity and stability, and have high degradation efficiency for methylene blue (MB) aqueous solution under light irradiation.

2. Experimental

2.1. Materials

$Zn(NO_3)_2 \cdot 6H_2O$ and CH_4N_2S were obtained from Alfa Aesar (Thermo Fisher Scientific, Ward Hill, MA, USA), while polyvinyl butyral (PVB) was obtained from Chang Chun Group Company (Kaohsiung, Taiwan) with an average molecular weight of approximately 40 kDa. Anhydrous ethanol (>99%) was supplied by PA Panreac (Barcelona, Spain). All chemicals were used in this experiment directly after purchase.

2.2. Preparation of PVB/ZnS composite nanofibers

In typical synthesis, a homogeneous PVB/ZnS precursor solution was prepared by dissolving 10 wt% PVB (ethanol/PVB ratio = 92:8), 2 mmol of zinc nitrate, and 16 mmol of thiourea in 10 mL of ethanol then magnetic stirring for 2 hours at room temperature. The

electrospinning setup included a high-voltage DC power supply capable of delivering up to 30 kV (You-Shang Technical Corp., Kaohsiung, Taiwan), a syringe pump (KD Scientific Inc., Holliston, USA), a syringe with a 0.21 mm internal diameter needle, and a collection board. The freshly prepared PVB/ZnS precursor solution was used for electrospinning immediately. The collected PVB/ZnS composite fibers were then calcined at 400 °C for 1 hour under a nitrogen (N_2) atmosphere.

2.3. Preparation of ZnS nanoparticles

In this study, the collected PVB/ZnS composite fibers were first dispersed in 24 mL of deionized (DI) water and then transferred into a 30 mL Teflon-lined stainless-steel autoclave until it was 80% full. The autoclave was subsequently heated at 140, 160, and 180 °C for 6 hours in an oven, respectively. After the heating process is completed, the autoclave is cooled naturally to room temperature. The resulting precipitates were washed and centrifuged multiple times with DI water and ethanol to remove any remaining solvent and by-products. Finally, the obtained products were dried at 80 °C for 6 hours.

2.4. Material characterization

The synthesized products were characterized using scanning electron microscopy (SEM), X-ray diffraction (XRD), transmission electron microscopy (TEM), and energy-dispersive X-ray spectroscopy (EDS). The particle morphology was examined via SEM (Hitachi 4200A, Japan) and FE-SEM (Hitachi S4800-I, Japan) at an operating voltage of 10 kV. XRD analysis was conducted using a Shimadzu XRD-6000 (Japan) equipped with a CuKα radiation source (λ = 0.15418 nm) operating at 40 kV. The measurements were performed over a 2θ range of 15° to 85° with a scanning rate of 0.03°/s. Detailed microstructural analysis was performed using TEM (JEOL JEM-2000EX, Japan), while the elemental composition of the particles was determined through EDS (Horiba EX220, Japan) integrated with the TEM system.

2.5. Photocatalytic performance

In this experiment, methylene blue (MB) dye was selected to evaluate the photocatalytic performance of the synthesized ZnS catalyst. The photocatalytic activity was assessed by degrading MB under visible light irradiation at room temperature. A xenon arc lamp (300W, Trusttech PLS-SXE 300, China) equipped with a UV-cut filter was used as the visible light source. For the photocatalytic test, 100 mg of the catalyst was dispersed in 100 mL of MB solution (20 mg/L) and stirred in the dark for 60 minutes to achieve adsorption equilibrium. The degradation efficiency of MB was monitored at specific time intervals using UV-visible spectroscopy. Based on Beer-Lambert's law, the concentration of the MB solution is directly proportional to its absorbance, enabling the degradation efficiency to be determined using the following formula: [44, 45]:

$$R = [C_0 - C)/C_0] \times 100\% = [A_0 - A)/A_0] \times 100\%$$

Among these, C_0 and C represent the concentration, while A_0 and A denote the absorbance of the MB aqueous solution at reaction times 0 and t, respectively.

3. Results and discussion

Figure 1 presents the SEM images of ZnS/PVB composite fibers synthesized under varying parameters. In Figure 1(a), the composite fiber prepared by 8 wt% PVB is quite thin, with a fiber diameter of about 100-150 nm, but a small amount of bead-like structure appears. In Figure 1(b), when the PVB concentration is 10wt%, ZnS/PVB composite fibers with smooth surfaces are obtained, and the fiber have the average diameter of 250±10nm. As the PVB concentration increases, the fiber diameter also increases, accompanied by the formation of bead-like structures. However, the density of these bead-like structures decreases. Figure 2(a) illustrates the effect of

varying PVB concentrations and flow rates on fiber diameter. The nanofibers exhibit an uneven diameter distribution with diameters range from 230 to 400 nm when a flow rate of 0.7 mL/h. Increasing the flow rate leads to a more uniform diameter distribution and an overall increase in the diameter of the ZnS/PVB composite fibers [46]. However, when the flow rate was too fast, exceeding 1.3 mL/h, the fiber thickness and diameter became inconsistent and irregular, and fibers tend to aggregate and adhere to neighboring fibers, as shown in Figure 1(c). In this case, fiber diameters vary significantly, ranging from approximately 200 to 700 nm. Based on these observations, the optimal flow rate for fabricating ZnS/PVB composite fibers is determined to be 1 mL/h.

The final investigation focused on the effect of applied voltage on fiber diameter. Figure 2(b) presents the impact of different applied voltages on fiber diameter at a fixed working distance of 5 cm and a flow rate of 1 mL/h. As the applied voltage increases from 12 kV to 16 kV, the diameter of ZnS/PVB composite fibers also increases. When the voltage is below 10 kV, fiber formation is not possible. This indicates that both excessively high and low operating voltages negatively affect fiber formation and morphology [46]. When Coulomb forces, viscoelastic forces, and surface tension reach equilibrium, a narrow fiber diameter distribution is achieved. Increasing the applied voltage enhances the Coulomb repulsion of the fluid jet, resulting in the formation of elongated fibers. However, further voltage increases strengthen the Coulomb force while reducing viscoelastic forces in the electrospun ZnS/PVB composite fibers, leading to overstretching and a higher likelihood of jet breakage during flight to the collection board. This part determined that the optimal applied voltage for producing ZnS/PVB composite fibers was 12 kV and the average fiber diameter was 145 nm.

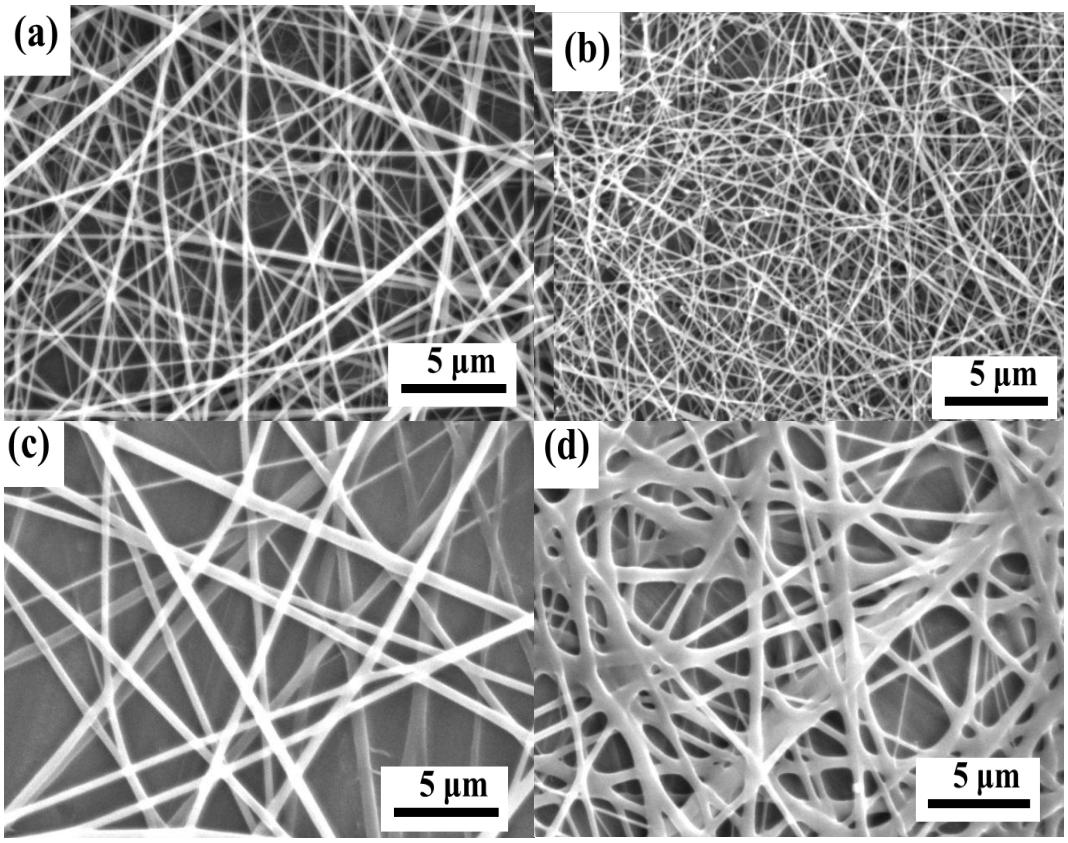

Fig. 1. The SEM images of PVB/ZnS composite fibers prepared with different PVB concentrations: (a) 8% and (b) 10%, as well as at varying precursor flow rates: (c) 1 mL/h and (d) 1.3 mL/h.

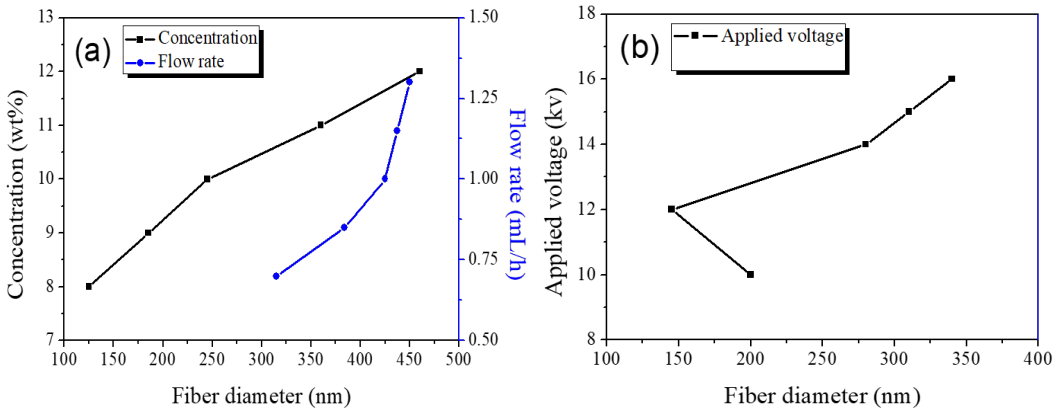

Fig. 2. (a) Diameter variations of PVB/ZnS composite fibers at different concentrations and flow rates, (b) Diameter changes of PVB/ZnS composite fibers under varying applied voltages.

Electrospun ZnS/PVB composite nanofibers are subsequently subjected to a hydrothermal process to obtain pure ZnS nanoparticles. Figure 3 shows the XRD analysis of as-electrospun ZnS/PVB composite fibers, and products of ZnS obtained by hydrothermal assisted electrospinning for 6 h at different reacting temperatures. The above results show that the prepared ZnS/PVB fiber is an amorphous phase, does not form a ZnS structure, and has poor crystallinity. Under hydrothermal treatment at 140 °C for 6 h, the ZnS structure was correct and visible crystallization occurred. As the temperature increased to 160 °C, all of the diffraction peaks match well with the standard data of sphalerite-type ZnS with cubic phase (JCPDS card No.05-0566) indicates that pure ZnS was synthesized.

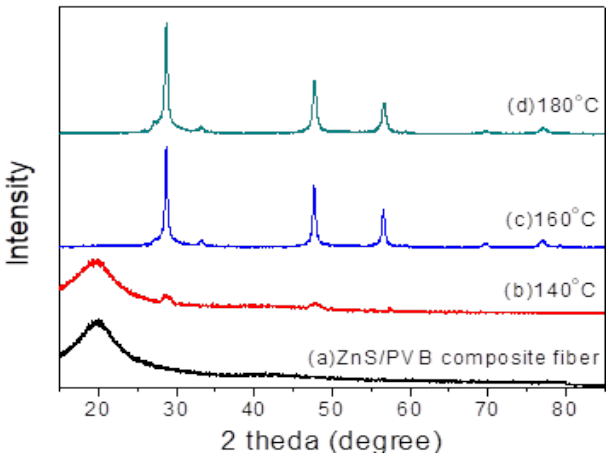

Fig. 3. XRD patterns of (a) PVB/ZnS composite fibers, and products of ZnS obtained by hydrothermal assisted electrospinning for 6 h at (b) 140 °C, (c) 160 °C, (d) 180 °C.

Figure 4 illustrates the process of placing the prepared ZnS/PVB composite fibers into a stainless-steel autoclave filled with deionized water for the hydrothermal treatment. The autoclave was then heated in an oven under the following conditions: (a) 140 °C for 6 hours, (b) 160 °C for 3 hours, (c) 160 °C for 6 hours, and (d) 180 °C for 6 hours. At relatively low reaction temperature of 140 °C, which supplies insufficient activation energy for ZnS synthesizing, resulting in that the ZnS/PVB composite nanofibers were covered by molten polymer film. When the reaction temperature was raised to 160°C for 3 hours, we could still observe a molten polymer film with some not easily observed particles on the film or cladded in the film. As the reaction time prolong

to 6 h, the sphere-shaped ZnS nanoparticles with crystal size about 200-250 nm can be obtained. In the reaction, the polymer cannot dissolve in water, therefore the Zn^{2+} and S^{2-} are cladded in electrospun nanofibers just like be restricted in polymer, as the result, Zn^{2+} and S^{2-} may be slowly released from ZnS/PVB composite nanofibers dissociated in the aqueous solutions. This process is opposite to normally hydrothermal reaction, the amount of precursor dissociated in autoclave at one time with high concentration precursor solution. The dissociated Zn^{2+} and S^{2-} further undergo crystallization of ZnS from high-temperature aqueous solutions at high vapor pressures. The advantage of slowly releasing the ions in solution is to control the ionic concentration in solution, anionic and cationic can effectively combine, so the size of the resulting nanoparticles may uniformly contain high crystallinity and with nanoscale. After completion of the reaction the polymer film will float on the surface of the solution. These series of reaction had been called "dissolution-recrystallization" mechanism. The EDS analysis showed that the molar ratio of Zn:S elements was 49.84:50.16. However, at high temperature of 180 °C, the formation size of ZnS nanoparticles is fairly non-uniform at the range of 300 nm, 800 nm and 1.2μm, which may be due to the reaction temperature is too high resulting in a fierce crystal growth process.

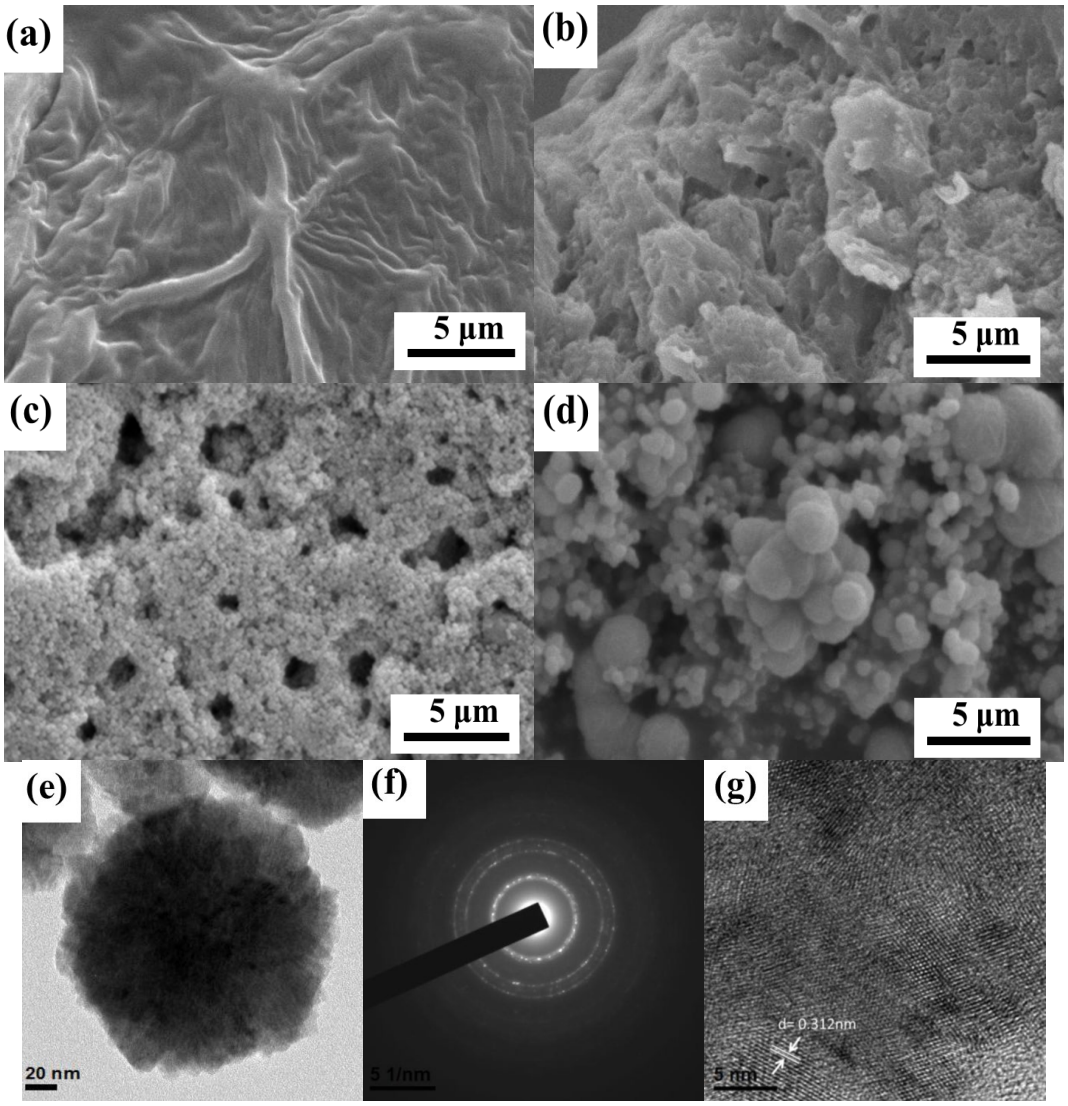

Fig. 4. The SEM images of products obtained by hydrothermal assisted electrospinning at (a)140℃ for 6h (b)160℃ for 3h, (c) 160℃ for 6h, (d)180℃ for 6h. The (e) TEM image (f) SAED pattern (g) HR-TEM image of ZnS obtained by hydrothermal assisted electrospinning route, and the reacting condition of hydrothermal process was 160 °C for 6 h.

The TEM image in Figure 4(e) further demonstrates the single sphere morphology of ZnS obtained by hydrothermal assisted electrospinning route, and the reacting condition of hydrothermal process was 160 °C for 6 h. The particle size of nanosphere was about 200nm, and with rough surface. The SAED pattern of the ZnS nanosphere is presented in Figure 4(f), showing the (111), (220), and (311) planes of cubic phase sphalerite ZnS, corresponding to JCPDS No. 05-0566, indicating that it has a polycrystalline structure. Figure 4(g) shows the high-resolution transmission electron microscopy (HR-TEM) image of ZnS nanospheres, revealing a lattice spacing of 0.312 nm, which matches the (111) lattice plane of ZnS.

In order to obtain nanoscale and high purity material, we tried the following three routes: calcination, hydrothermal, and hydrothermal assisted electrospinning. To understand and prove that the hydrothermal assisted electrospinning in this study is the best method to obtain high purity material with nanoscale, we will compare this method with calcination and hydrothermal process. Figure 5 show the SEM images and XRD patterns of ZnS obtained by (a) calcination, (b) hydrothermal assisted electrospinning route, (c) hydrothermal, respectively. From SEM image the particle size of ZnS obtained by using electrospun PVB/ZnS composite fibers further calcination and the ZnS obtained by hydrothermal assisted electrospinning route are about the same size, about 200-300 nm. Moreover, although the size of the ZnS obtained by calcination and hydrothermal assisted electrospinning route are almost the same, but particle size getting from hydrothermal assisted electrospinning show higher uniformity. On the other hand, the particle size of ZnS obtained by only hydrothermal process is approximately 3-5μm which is larger than the particle size gotten from hydrothermal assisted electrospinning. From the XRD pattern, the ZnS particles prepared by the hydrothermal method and the hydrothermal method assisted electrospinning method have higher purity, but the ZnS prepared by the calcination method has other impurities. The difference between hydrothermal assisted electrospinning and hydrothermal process is that the amount of sulfide ion released in solution. It had been reported that excess thiourea will help the crystal growth of wurtzite in hydrothermal reaction [47]. This result also proved that the zinc ions sulfide ions are truly cladded in polymer as composite fibers limit the ability to outward dissolution then slowly release to conduct dissolution-recrystallization reaction. The final results showed that the hydrothermal assisted electrospinning method follows the dissolution-recrystallization mechanism can synthesize nanoscale and high-purity materials.

To assess the photocatalytic performance of ZnS particles, we studied the degradation efficiency under visible light irradiation of MB aqueous solutions. The ZnS particles (100 mg/L) obtained by calcination, hydrothermal, and hydrothermal assisted electrospinning under visible light are also shown in Figure 6 as a comparison. We observe that when no catalyst is used, the MB solution hardly decolorizes under visible light irradiation. However, as the exposure time increases, the MB solution can still be gradually photocatalytically degraded (i.e., its concentration decreases). The degradation efficiency of ZnS particlesby calcination and hydrothermal reached 73%, and 45%, respectively. However, the degradation efficiency for ZnS nanoparticles synthesis by hydrothermal assisted electrospinning reached 90% after 3 h, which shows significant improvement in photo catalytic activity as compared to other conditions. This result indicates that the high crystallinity ZnS nanoparticles exhibited greater activity than that of ZnS obtained from calcination or hydrothermal route. It is not only due to the higher surface to volume ratio in nanosize ZnS, but also due to the significant reduced recombination of the electron–hole pair within the semiconductor particle because of the high crystallinity. This means that dissolution-recrystallization mechnism would provide a tremendous specific surface area and less recombination center for more effective photocatalytic degradation.

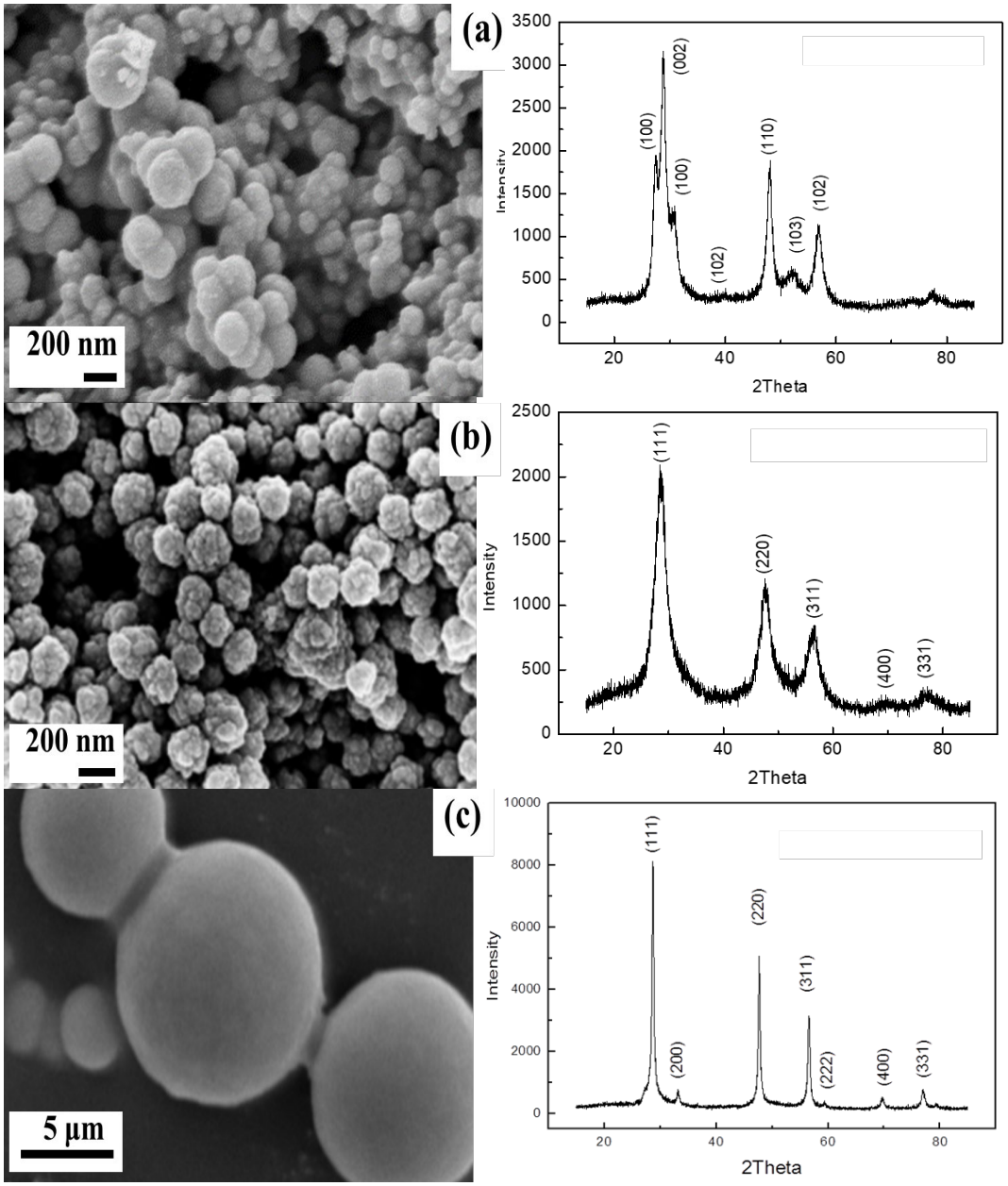

Fig. 5. The SEM images and XRD patterns of ZnS obtained by (a) calcination, (b) hydrothermal assisted electrospinning route, (c) hydrothermal, respectively.

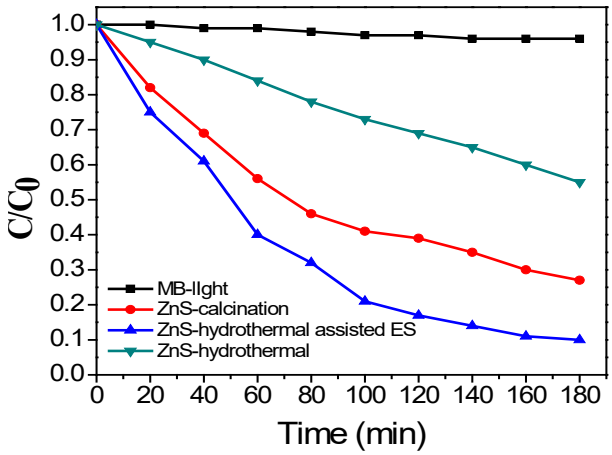

Fig. 6. The SEM images and XRD patterns of ZnS obtained by (a) calcination, (b) hydrothermal assisted electrospinning route, (c) hydrothermal, respectively.

4. Conclusion

In summary, we are successful to obtain ZnS nanospheres with nanoscale and high crystallinity quality via dissolution-recrystallization mechanism by hydrothermal assisted electrospinning route. The calcined and hydrothermal assisted electrospun ZnS nanoparticles showed sphere-shaped and the particle size is about 200-300 nm with cubic structure; on the other hand, the ZnS obtained by hydrothermal have a hexagonal structure with diameters about 3-5μm. As the results have shown, the degradation efficiency for hydrothermal assisted electrospun ZnS nanoparticle was 90%. The degradation ability was increased by high surface area and less recombination center, contributed by nanoscale and high crystallinity quality of photocatalyst ZnS. The photocatalytic degradation on methyl blue illustrates that ZnS nanoparticles synthesized by this novel technique could be used as a promising catalytic degradation material.

Acknowledgements

The authors partially acknowledge the support of the National Science and Technology Council, Taiwan, under grant number NSTC 113-2222-E-992-008.

References

[1] Y. K. Syue, K. C. Hsu, T. H. Fang, C. I. Lee, C. J. Shih, Ceram. Int. 48, 12585-12591 (2022); https://doi.org/10.1016/j.ceramint.2022.01.126

[2] V. Gurylev, T. P. Perng, J. Eur. Ceram. Soc. 41, 4977-4996 (2021); https://doi.org/10.1016/j.jeurceramsoc.2021.03.031

[3] K. C. Hsu, T. H. Fang, S. H. Chen, E. Y. Kuo, Ceram. Int. 45, 8744-8749 (2019); https://doi.org/10.1016/j.jallcom.2020.157014

[4] K. C. Hsu, T. H. Fang, Y. J. Hsiao, P. C. Wu, J. Alloys Compd. 794, 576-584 (2019); https://doi.org/10.1016/j.jallcom.2019.04.238

[5] A. M. Ruiz, G. Sakai, A. Cornet, K. Shimanoe, J. R. Morante, N. Yamazoe, Sens. Actuators B Chem. 93, 509-518 (2003); https://doi.org/10.1016/S0925-4005(03)00183-7

[6] P. M. Perillo, D. F. Rodríguez, J. Alloys Compd. 657, 765-769 (2016); https://doi.org/10.1016/j.jallcom.2015.10.167

[7] T. Y. Lai, T. H. Fang, Y. J. Hsiao, C. A. Chan, Vacuum. 166, 155-161 (2019); https://doi.org/10.1016/j.vacuum.2019.04.061

[8] K. C. Hsu, T. H. Fang, Y. J. Hsiao, C. A. Chan, Mater. Lett. 261, 127144 (2020); https://doi.org/10.1016/j.matlet.2019.127144

[9] W. Zhang, B. Yang, J. Liu, X. Chen, X. Wang, C. Yang, Sens. Actuators B Chem. 243, 982-989 (2017); https://doi.org/10.1016/j.snb.2016.12.095

[10] K. C. Hsu, B. D. Chen, T. H. Fang, C. M. Hsu, Ceram. Int. 49, 2236-2243 (2023); https://doi.org/10.1016/j.ceramint.2022.09.191

[11] M. Righettoni, A. Tricoli, S. Gass, A. Schmid, A. Amann, S. E. Pratsinis, Anal. Chim. Acta. 738, 69-75 (2012); https://doi.org/10.1016/j.aca.2012.06.002

[12] K. Anand, J. Kaur, R. C. Singh, R. Thangaraj, Chem. Phys. Lett. 682, 140-146 (2017); https://doi.org/10.1016/j.cplett.2017.06.008

[13] K. C. Hsu, T. H. Fang, I. T. Tang, Y. J. Hsiao, C. Y. Chen, J. Alloys Compd. 822, 153475 (2020); https://doi.org/10.1016/j.jallcom.2019.153475

[14] K. Qiu, D. Qiu, L. Cai, S. Li, W. Wu, Z. Liang, H. Shen, Mater. Lett. 198, 23-26 (2017); https://doi.org/10.1016/j.matlet.2017.03.171

[15] R. H. Castillo, M. Acosta, I. Riech, G. S. Rodríguez, J. M. Gamboa, C. Acosta, M. Zambrano, Optik 148, 95-100 (2017); https://doi.org/10.1016/j.ijleo.2017.09.002

[16] H. Li, X. Liu, Solar Energy, 115, 603-612 (2015); https://doi.org/10.1016/j.solener.2015.02.044

[17] Y. Bacherikov, A. Kuchuk, A. Zhuk, Y. Polischuk, V. Kladko, T. Kryshtab, N. Korsunska, J. Lumin, J. Lumin. 145, 970-975 (2014); https://doi.org/10.1016/j.jlumin.2013.09.030

[18] A. R. Mirhabibi, M. Rabiee, R. Aghababazadeh, F. Moztarzadeh, S. Hesaraki, Pigm. Resin Technol. 32, 358-363 (2003); https://doi.org/10.1108/03699420310507803

[19] T. K. Tran, W. Park, W. Tong, M. M. Kyi, B. K. Wagner, C. J. Summers, J. Appl. Phys. 81, 2803-2809 (1997); https://doi.org/10.1063/1.363937

[20] H. C. Ong, R. P. H. Chang, Appl. Phys. Lett. 79, 3612-3614 (2001); https://doi.org/10.1063/1.1419229

[21] M. Ihara, T. Igarashi, T. Kusunoki, K. Ohno, J. Electrochem. Soc. 149, H72 (2002); https://doi.org/10.1149/1.1447226

[22] Y. Li, Y. Ding, Y. Zhang, Y. Qian, J. Phys. Chem. Solids 60, 13-15 (1999);

https://doi.org/10.1016/S0022-3697(98)00247-9

[23] S. Shionoya, Phosphor Handbook, CRC Press LLC, New York, U.S.A (1999).

[24] W. Park, B. K. Wagner, G. Russell, K. Yasuda, C. J. Summers, Y. R. Do, H. G. Yang, J. Mater. Res. 15, 2288-2291 (2000); https://doi.org/10.1557/JMR.2000.0328

[25] K. V. V. Satyanarayana, M. R. Chandra, P. A. Ramaiah, Y. L. N. Murty, E. N. Pandit, S. V. N. Pammi, Inorg. Chem. Front. 1, 306-310 (2014) https://doi.org/10.1039/c3qi00016h

[26] D. H. Hwang, J. H. Ahn, K. N. Hui, K. S. Hui, Y. G. Son, Nanoscale Res Lett. 7, 26-32 (2012); https://doi.org/10.1186/1556-276X-7-26

[27] S. P. Patel, J. C. Pivin, V. V. S. Kumar, A. Tripathi, D. Kanjilal, L. Kumar, Vacuum, 85, 307-311 (2010); https://doi.org/10.1016/j.vacuum.2010.06.011

[28] S. P. Patel, A. K. Chawla, R. Chandra, J. Prakash, P. K. Kulriya, J. C. Pivin, D. Kanjilal, L. Kumar, Solid State Commun. 150, 1158-1161 (2010); https://doi.org/10.1016/j.ssc.2010.03.017

[29] N. Roy, A. Roy, J. Mater. Sci: Mater Electron, 25, 1275-1279 (2014); https://doi.org/10.1007/s10854-014-1721-9

[30] A. Goudarzi, G. M. Aval, R. Sahraei, H. Ahmadpoor, Thin Solid Films, 516, 4953-4957 (2008); https://doi.org/10.1016/j.tsf.2007.09.051

[31] L. X. Shao, K. H. Chang, H. L. Hwang, Appl. Surf. Sci. 212-213, 305-310 (2003); https://doi.org/10.1016/S0169-4332(03)00085-0

[32] K. Tomita, V. Petrykin, M. Kobayashi, M. Shiro, M. Yoshimura, M. Kakihana, Angew. Chem., Int. Ed. 45, 2378-2381 (2006); https://doi.org/10.1002/anie.200503565

[33] Y. Li, T. Zhang, S. Fan, G. Cheng, Opt. Mater. 66, 356-360 (2017); https://doi.org/10.1016/j.optmat.2017.02.019

[34] Q. Li, C. Wang, Appl. Phys. Lett. 83, 359-361 (2003); https://doi.org/10.1063/1.1591999

[35] S. Mandal, S. I. Ali, A. C. Mandal, Appl. Phys. A 129, 219 (2023); https://doi.org/10.1007/s00339-023-06499-z

[36] D. Lin, H. Wu, R. Zhang, W. pan, J. Am. Ceram. Soc. 90, 3664-3666 (2007); https://doi.org/10.1111/j.1551-2916.2007.01942.x

[37] H. M. Hussein, Colloid J. 85, 666-672 (2023); https://doi.org/10.1134/S1061933X22600610

[38] Z. Li, B. Liu, X. Li, S. Yu, L. Wang, Y. Hou, Y. Zou, M. Yao, Q. Li, B. Zou, T.Cui, G. Zou, G. Wang, Y. Liu, Nanotechnology 18, 255602 (2007); https://doi.org/10.1088/0957-4484/18/25/255602

[39] H. Liu, Y. Ni, M. Han, Q. Liu, Z. Xu, J. Hong, X. Ma, Nanotechnology 16, 2908-2912

(2005); https://doi.org/10.1088/0957-4484/16/12/030

[40] S. Biswas, S. Kar, Nanotechnology 19, 045710-045720 (2008); https://doi.org/10.1088/0957-4484/19/04/045710

[41] L. Chai, J. Du, S. Xiong, H. Li, Y. Zhu, Y. Qian, J. Phys. Chem. C 111, 12658-12662 (2007); https://doi.org/10.1021/jp073009x

[42] Z. Zhou, D. He, W. Xu, F. Ren, Y. Qian, Mater. Lett. 61, 4500-4503 (2007); https://doi.org/10.1016/j.matlet.2007.02.041

[43] M. H. Chiang, W. T. Lin, B. S. Wang, K. C. Hsu, Y. S. Fu, Ceram. Int. 43, 5819-5822 (2017); https://doi.org/10.1016/j.ceramint.2017.01.063

[44] W. J. Chen, K. C. Hsu, T. H. Fang, C. I. Lee, T. H. Chen, T. H. Hsieh, Digest J. Nanomater. Biostruct. 16, 1227-1234 (2021); https://doi.org/10.15251/DJNB.2021.164.1227

[45] K. C. Hsu, T. H. Fang, C. I. Lee, T. H. Chen, T. H. Hsieh, Top. Catal. 63, 956-963 (2020); https://doi.org/10.1007/s11244-020-01300-4

[46] K. C. Hsu, J. D. Liao, J. R. Yang, Y. S. Fu, CrystEngComm 15, 4303-4308 (2013); https://doi.org/10.1039/c3ce00052d

[47] X. Chen, H. Xu, N. Xu, F. Zhao, W. Lin, G. Lin, Y. Fu, Z. Huang, H. Wang, M. Wu, Inorg. Chem. 42, 3100-3106 (2003); https://doi.org/10.1021/ic025848y